Generalized Su-Schrieffer-Heeger Model in One Dimensional Optomechanical Arrays

Xun-Wei Xu[1,2]*, Yan-Jun Zhao[3], Hui Wang[4], Ai-Xi Chen[5]* and Yu-Xi Liu[6,7]

[1]Key Laboratory of Low-Dimensional Quantum Structures and Quantum Control of Ministry of Education, Key Laboratory for Matter Microstructure and Function of Hunan Province, Department of Physics and Synergetic Innovation Center for Quantum Effects and Applications, Hunan Normal University, Changsha, China, [2]Department of Applied Physics, East China Jiaotong University, Nanchang, China, [3]Key Laboratory of Opto-electronic Technology, Ministry of Education, Beijing University of Technology, Beijing, China, [4]Inspur Academy of Science and Technology, Jinan, China, [5]Department of Physics, Zhejiang Sci-Tech University, Hangzhou, China, [6]Institute of Microelectronics, Tsinghua University, Beijing, China, [7]Beijing National Research Center for Information Science and Technology (BNRist), Beijing, China

We propose an implementation of a generalized Su-Schrieffer-Heeger (SSH) model based on optomechanical arrays. The topological properties of the generalized SSH model depend on the effective optomechanical interactions which can be controlled by strong driving fields. Three phases including one trivial and two distinct topological phases are found in the generalized SSH model. The phase transition can be observed by turning the strengths and phases of the effective optomechanical interactions *via* adjusting the driving fields. Moreover, four types of edge states can be created in generalized SSH model of an open chain under single-particle excitation, and the dynamical behaviors of the excitation in the open chain are related to the topological properties under the periodic boundary condition. We show that the edge states can be pumped adiabatically along the optomechanical arrays by periodically modulating the amplitude and frequency of the driving fields, and the state pumping is robust against small disorders. The generalized SSH model based on the optomechanical arrays provides us a controllable platform to engineer topological phases for photons and phonons, which may have potential applications in controlling the transport of photons and phonons.

Keywords: optomechanical arrays, generalized Su-Schrieffer-Heeger model, topological phases, edge states, adiabatic particle pumping

1 INTRODUCTION

In the past decades, rapid progress has been made in the field ofcavity optomechanical systems, in which a cavity mode is coupled to a mechanical mode *via* radiation pressure or optical gradient force (for reviews, see Refs. [1–6]). With the advance in technology and the requirement for providing new functionality, the focus has been changed from the simplest optomechanical systems, based on a single mechanical mode coupled to a single optical mode, to more complex setups, including many optical or mechanical modes, such as optomechanical arrays, which are designed as a periodic arrangement of optomechanical systems. Based on the current condition of experiments and technology, optomechanical arrays might be realized in coupled optical microdisks [7–10], on-chip superconducting electromechanical cavity arrays [11–14], and optomechanical crystals [15, 16].

In the past few years, quantum many-body effect in optomechanical arrays has attracted considerable attentions [17–32]. Optomechanical arrays with parametric coupling between the

mechanical mode and optical mode provide us a controllable platform to simulate quantum many-body systems and manipulate photons and phonons. Many interesting phenomena have been studied, such as controllable photon propagation [17, 18], synchronization [19–21], artificial magnetic fields for photons [22], optically tunable Dirac-type band structure [23, 24], Anderson localization of hybrid photon-phonon excitations [25, 26], and Kuznetsov-Ma soliton [27]. Besides these, the optomechanical arrays can also be used to engineer topological phase for both photons and phonons [28–32].

Most of the optomechanical arrays, which are used to demonstrate different topological phases and Chern insulators, are implemented in two-dimensional optomechanical crystals. However, two dimension is not a necessary condition for engineering topological phase. The topological properties of photons and phonons can also be realized in a one-dimensional chain of optomechanical cavities. For example, in the recent works, Z_2 topological insulators [33] and Kitaev model [34] were simulated via one-dimensional optomechanical arrays.

The Su-Schrieffer-Heeger (SSH) model, introduced from polyacetylene [35], is well known as one of the simplest models to demonstrate topological character in one dimension. It has been proposed theoretically and demonstrated experimentally in many different setups, such as cold atoms and ions [36–46], optical systems [47–51], mechanical systems [52–54], heterostructure [55], graphene nanoribbons [56], plasmonic systems [57–63], and superconducting circuits [64–71]. In addition, ladder systems, which consist of two or more coupled SSH chains, have been used to demonstrate richer topological quantum phases [72–77].

In this paper, we study the topological properties of a one-dimensional optomechanical array, which can be mapped to a generalized SSH model [78–85] including three complex hopping amplitudes. Different from the standard SSH model, we find that there are three phases in this generalized SSH model, among which, one is trivial and the other two are distinct. It is worth mentioning that a SSH model consisting of three hopping amplitudes with real numbers was discussed in a recent Ref. [77]. Besides the system in our paper is different from that in Ref. [77], we further show that the topological properties of the generalized SSH model depend on both the strengths and the phases of the hopping amplitudes, and topological phase transitions can be demonstrated by tuning the strengths and phases of the effective optomechanical interactions via adjusting the external driving fields. Moreover, we show that four types of edge states can be found in generalized SSH model of an open chain under single-particle excitation, and the dynamical behaviors of the excitation in the open chain are related to topological properties under the periodic boundary condition. We also show that the edge states can be pumped adiabatically along the optomechanical arrays by periodically modulating the amplitudes and frequencies of the driving fields.

It is worth mentioning that, after the submission of the first version of this manuscript to arXiv [86], there are many new advances have been made in the field of topological phases in optomechanical arrays based on SSH model, such as topological

state transfer and topological beam splitter [87], photon-phonon conversion [88], etc. Moreover, topological insulator in two synthetic dimensions was proposed based on an optomechanical resonator [89], and phononic edge modes with unidirectional propagation was simulated in a two-dimensional optomechanical nanobeam lattice [90].

The remainder of this paper is organized as follows. In **Section 2**, we show the theoretical model of a generalized SSH model based on optomechanical arrays. In **Section 3**, we study the topological properties of the generalized SSH model and show that there are three phases, one is trivial and two are distinct. Moreover, we show that phase transitions can be observed by tuning the strengths of the optomechanical interactions. In **Section 4**, four types of edge states are introduced and the relation between the dynamical behaviors of singleparticle excitation in the open chain and the topological properties under the periodic boundary condition are discussed. In **Section 5**, we demonstrate that the edge states can be pumped adiabatically along the optomechanical arrays by modulating the amplitudes and frequencies of the driving fields periodically. Finally, the results are summarized in **Section 6**.

2 THEORETICAL MODEL

We propose to implement a generalized SSH model by an optomechanical array with N cavity modes and N mechanical modes, which are coupled only by optomechanical interactions, without hopping of photons between neighboring cavity modes (or hopping of phonons between mechanical modes). The Hamiltonian of the optomechanical array is ($\hbar = 1$)

$$H_0 = \sum_{j=1}^{N} \left(\omega_{c,j} a_j^\dagger a_j + \omega_{m,j} b_j^\dagger b_j + H_j \right), \tag{1}$$

with

$$H_1 = \left[\left(g_{1,0} b_1^\dagger + g_{1,+} b_2^\dagger \right) a_1^\dagger a_1 \right. \\ \left. + \left(\Omega_{1,0} e^{i\omega_{1,0} t} + \Omega_{1,+} e^{i\omega_{1,+} t} \right) a_1 \right] + \text{H.c.,} \tag{2}$$

for the first cavity mode,

$$H_N = \left[\left(g_{N,0} b_N^\dagger + g_{N,-} b_{N-1}^\dagger \right) a_N^\dagger a_N \right. \\ \left. + \left(\Omega_{N,0} e^{i\omega_{N,0} t} + \Omega_{N,-} e^{i\omega_{N,-} t} \right) a_N \right] + \text{H.c.,} \tag{3}$$

for the last cavity mode, and

$$H_j = \left[\left(g_{j,0} b_j^\dagger + g_{j,+} b_{j+1}^\dagger + g_{j,-} b_{j-1}^\dagger \right) a_j^\dagger a_j \right. \\ \left. + \left(\Omega_{j,0} e^{i\omega_{j,0} t} + \Omega_{j,+} e^{i\omega_{j,+} t} + \Omega_{j,-} e^{i\omega_{j,-} t} \right) a_j \right] \\ \left. + \text{H.c.,} \right. \tag{4}$$

for the jth cavity mode ($1 < j < N$), where a_j ($a_j^\dagger$) is the bosonic annihilation (creation) operator of the jth cavity mode ($j = 1$, 2, . . . , N) with resonant frequency $\omega_{c,j}$, b_j ($b_j^\dagger$) is the bosonic annihilation (creation) operator of the jth mechanical mode with resonant frequency $\omega_{m,j}$, and $g_{j,0}$ ($g_{j,\pm}$) is the optomechanical coupling strength between the jth cavity mode and the jth mechanical mode (the $(j \pm 1)$th mechanical mode). The jth

cavity mode is driven by a three-tone laser at frequencies $\omega_{j,0} = \omega_{c,j} - \omega_{m,j}$ and $\omega_{j,\pm} = \omega_{c,j} - \omega_{m,j\pm1}$ with amplitudes $\Omega_{j,0}$ and $\Omega_{j,\pm}$ in the well resolved sidebands regime ($\omega_{m,j} \gg \{\kappa_j, \gamma_j\}$), where κ_j is the decay rate of the jth cavity mode, and γ_j is the damping rate of the jth mechanical mode).

To deal with the Hamiltonians in **Eqs 2–4**, we will employ the linearization approach widely used for optomechanics [91–96] in the weak single-photon optomechanical coupling regime and under strong driving condition $g_{j,\sigma} \ll \kappa_j \ll \Omega_{j,\sigma}$ ($\sigma = 0, \pm$). The operator for each cavity modes is written as the sum of its classical mean value $\alpha_j(t)$ and quantum fluctuation operator δa_j as $a_j \rightarrow \alpha_j(t) + \delta a_j$. For convenience of the presentation, we rename $\delta a_j \rightarrow a_j$. The classical mean value $\alpha_j(t)$ can be given approximately as $\alpha_j(t) \approx \alpha_{j,0}e^{i\omega_{j,0}t} + \alpha_{j,+}e^{i\omega_{j,+}t} + \alpha_{j,-}e^{i\omega_{j,-}t}$, where the classical amplitude $\alpha_{j,0} \approx -i2\Omega_{j,0}/(\kappa_j + 2i\Delta_{j,0})$ [$\alpha_{j,\pm} \approx -i2\Omega_{j,\pm}/(\kappa_j + 2i\Delta_{j,\pm})$] is given approximately by solving the classical equation of motion with amplitude $\Omega_{j,0}$ ($\Omega_{j,\pm}$) and detuning $\Delta_{j,0} \equiv \omega_{c,j} - \omega_{j,0}$ ($\Delta_{j,\pm} \equiv \omega_{c,j} - \omega_{j,\pm}$). In the interaction picture with respect to $H_{\mathrm{rot}} = \sum_{j=1}^N [\omega_{c,j}a_j^\dagger a_j + \omega_{m,j}b_j^\dagger b_j]$, the linearized operator a_j is given by

$$a_j \rightarrow a_j e^{i\omega_{c,j}t} + \sum_{\sigma=0,\pm} \alpha_{j,\sigma}e^{i\omega_{j,\sigma}t}. \tag{5}$$

We assume: 1) $\min[|\alpha_{j,0}|, |\alpha_{j,\pm}|] \gg 1$ and $\max\{g_{j,0}, g_{j,\pm}\} \ll \kappa_j$, so that we can only keep the first-order terms in the small quantum fluctuation operators a_j and $a_j^\dagger$ as

$$a_j^\dagger a_j \rightarrow a_j^\dagger \sum_{\sigma=0,\pm} \alpha_{j,\sigma}e^{i\Delta_{j,\sigma}t} + \mathrm{H.c.}. \tag{6}$$

2) $\min\{\omega_{m,j}, |\omega_{m,j} - \omega_{m,j'}|_{j'=j\pm1}\} \gg \max\{|g_{j,0}\alpha_{j,0}|, |g_{j,\pm}\alpha_{j,\pm}|\}$, and $\omega_{m,j} = \omega_{c,j} - \omega_{j,0}$ and $\omega_{m,j\pm1} = \omega_{c,j} - \omega_{j,\pm}$, such that the rotating terms can be neglected safely, and the linearized Hamiltonian with resonant interactions is obtained as

$$H_j \approx Je^{i\phi}a_j^\dagger b_j + za_j^\dagger b_{j+1} + va_j^\dagger b_{j-1} + \mathrm{H.c.}, \tag{7}$$

where $Je^{i\phi} \equiv g_{j,0}\alpha_{j,0}$, $v \equiv g_{j,-}\alpha_{j,-}$, and $z \equiv g_{j,+}\alpha_{j,+}$. We assume that the strengths ($\Omega_{j,0}, \Omega_{j,\pm}$) and detunings ($\Delta_{j,0}, \Delta_{j,\pm}$) of the driving fields are constant (or change slowly in the Section for adiabatic particle pumping), so the classical amplitudes ($\alpha_{j,0}, \alpha_{j,\pm}$) are constant in the steady state (or change slowly for adiabatic particle pumping). In this case, the classical mean value can be used as a parameter to define J, ϕ, v and z in the Hamiltonians. Without loss of generality, we assume that J, ϕ, v and z are real numbers and the global phase factor ϕ can be tuned by adjusting the relative phase of the driving fields. It should be noted that all these assumptions given above are widely used in the theories for optomechanical systems [4], including in one- and two-dimensional optomechanical lattices [28–34, 87–90].

By substituting **Eq. 7** into **Eq. 1**, the linearized Hamiltonian for the optomechanical array in the interaction picture with respect to $H_{\mathrm{rot}} = \sum_{j=1}^N [\omega_{c,j}a_j^\dagger a_j + \omega_{m,j}b_j^\dagger b_j]$ is given by

$$H = \sum_{j=1}^N Je^{i\phi}a_j^\dagger b_j + \sum_{j=1}^{N-1}\left(va_{j+1}^\dagger b_j + zb_{j+1}^\dagger a_j\right) + \mathrm{H.c.}, \tag{8}$$
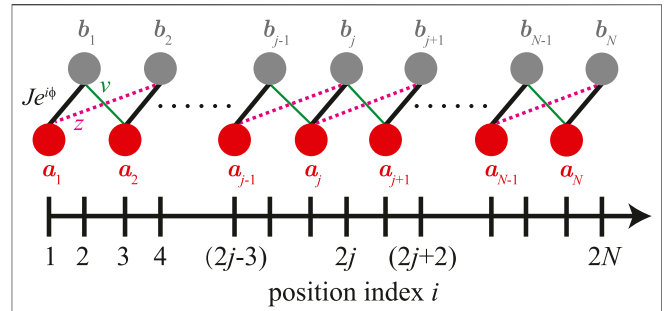

FIGURE 1 | (Color online) Schematic diagram of a generalized SSH model based on an optomechanical array. a_j and b_j denote the cavity and mechanical modes respectively, and they are coupled with three different hopping amplitudes $Je^{i\phi}$ (bold black lines), v (thin green lines) and z (red dashed lines). The optomechanical array can be implemented by an array of coupled optical microdisks [7–10], on-chip superconducting circuit electromechanical cavities [11–14], and optomechanical crystals [15, 16].

as schematically shown in **Figure 1**. The linearized Hamiltonian for the optomechanical array shows a generalized SSH model with hopping amplitude $z \neq 0$ between the jth cavity mode and $(j + 1)$th mechanical mode. When the coupling strength $z = 0$, the Hamiltonian for the optomechanical array becomes the well-known SSH model [78]. It can also be dealt with as a Bogoliubov Hamiltonian if the counter-rotating terms, $\zeta a_{j+1}b_j + \zeta' a_j b_{j+1} + \mathrm{H.}$ c. with coupling strengths ζ and ζ', are taken into account [41, 42].

3 TOPOLOGICAL PHASE TRANSITION

To study the topological phase transition in the generalized SSH model, we set a periodic boundary condition, so the linearized Hamiltonian for one-dimensional optomechanical array can be redefined as

$$H' = \sum_{j=1}^N \left(Je^{i\phi}a_j^\dagger b_j + va_{(j\,mod\,N)+1}^\dagger b_j + zb_{(j\,mod\,N)+1}^\dagger a_j\right) + \mathrm{H.c.}, \tag{9}$$

where "mod" stands for the modular calculation. By using the discrete Fourier transform for a_j and b_j as

$$\begin{pmatrix} a_j \\ b_j \end{pmatrix} = \sum_k e^{-ikj}\begin{pmatrix} a_k \\ b_k \end{pmatrix}, \tag{10}$$

then the Hamiltonian in **Eq. 9** can be rewritten as

$$H' = \sum_k \begin{pmatrix} a_k^\dagger & b_k^\dagger \end{pmatrix} H'(k)\begin{pmatrix} a_k \\ b_k \end{pmatrix} \tag{11}$$

with

$$H'(k) = \begin{pmatrix} 0 & h(k) \\ h^\star(k) & 0 \end{pmatrix} \tag{12}$$
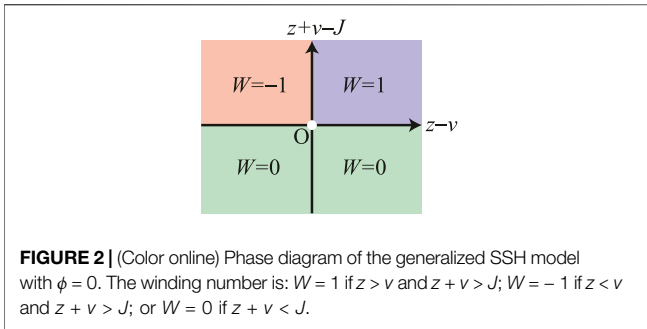
and

FIGURE 2 | (Color online) Phase diagram of the generalized SSH model with $\phi = 0$. The winding number is: $W = 1$ if $z > v$ and $z + v > J$; $W = -1$ if $z < v$ and $z + v > J$; or $W = 0$ if $z + v < J$.

$$h(k) = Je^{i\phi} + ve^{-ik} + ze^{ik}, \quad (13)$$

where k is the wavenumber in the first Brillouin zone. The dispersion relation of the generalized SSH model with periodic boundary conditions is given by

$$E = \pm|Je^{i\phi} + ve^{-ik} + ze^{ik}|. \quad (14)$$

The topological invariant of an insulating Hamiltonian can be characterized by the dispersion relation and the winding numbers W defined by [77, 78].

$$W = \frac{1}{2\pi i}\int_{-\pi}^{\pi} dk \frac{d\ln h(k)}{dk}. \quad (15)$$

For the generalized SSH model with $h(k)$ given by **Eq. 13**, the winding number is either 0 or ± 1, depending on the parameters J, ϕ, z and v. The phase diagram is shown in **Figure 2**. When the phase factor $\phi = 0$, the winding number is: 1) $W = 1$ if $z > v$ and $z + v > J$; 2) $W = -1$ if $z < v$ and $z + v > J$; 3) $W = 0$ if $z + v < J$.

The Hamiltonian for the generalized SSH model in the momentum space can be written in an alternative form as

$$H'(k) = \mathbf{d}(k) \cdot \hat{\sigma}$$
$$= d_x(k)\hat{\sigma}_x + d_y(k)\hat{\sigma}_y + d_z(k)\hat{\sigma}_z, \quad (16)$$

where $\hat{\sigma}_x$, $\hat{\sigma}_y$, and $\hat{\sigma}_z$ are the Pauli matrices, and

$$d_x(k) = J\cos\phi + v\cos k + z\cos k, \quad (17)$$
$$d_y(k) = J\sin\phi - v\sin k + z\sin k, \quad (18)$$
$$d_z(k) = 0. \quad (19)$$

The winding number can also be obtained graphically by counting the number of times the loop winds around the origin of the d_x, d_y plane.

We show the dispersion relation and the path that the endpoint of the vector $\mathbf{d}(k)$ traces out in **Figure 3** for $v > z$. As the wavenumber runs through the Brillouin zone, $k = 0 \to 2\pi$, the path that the endpoint of the vector $\mathbf{d}(k)$ is a closed ellipse of long axis $v + z$ and short axis $|v - z|$ on the d_x, d_y plane, centered at $(J, 0)$, and the endpoint rotates around the origin clockwise. It is clear that the winding number is $W = -1$ when $z + v > J$ for $z < v$, and the winding number is $W = 0$ when $z + v < J$.

Two more figures about the dispersion relation and the path that the endpoint of the vector $\mathbf{d}(k)$ traces are shown in **Supplementary Figures S1, S2** in the supplementary material [97]. As $v = z$, the path of the endpoint of the vector $\mathbf{d}(k)$ becomes a straight line on the d_x-axis. As $v < z$, similarly to the case for $v > z$, the path of the endpoint of the vector $\mathbf{d}(k)$ is also a closed ellipse of long axis $v + z$ and short axis $|v - z|$ on the d_x, d_y plane, centered at $(J, 0)$. However, the endpoint rotates around the origin counterclockwise for $v < z$. So we can conclude that the winding number is 1) $W = 1$ when $z + v > J$ and $v < z$; 2) $W = -1$ when $z + v > J$ and $v > z$; 3) $W = 0$ when $z + v < J$. These consist with the results shown in **Figure 2**.

The above results are obtained under the condition for $\phi = 0$. In **Figure 4**, we show that the topological phase transition can be induced by tuning the phase ϕ. For $\phi \neq 0$, the path that the endpoint of the vector $\mathbf{d}(k)$ is centered at $(J\cos\phi, J\sin\phi)$, so the
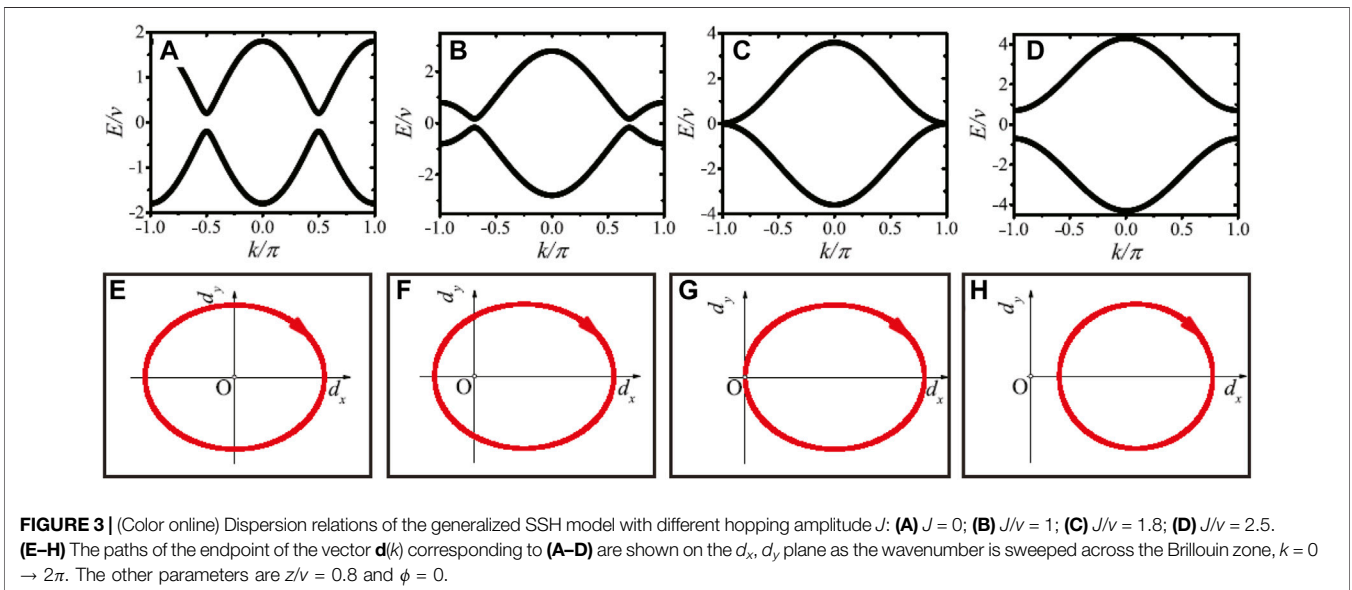

FIGURE 3 | (Color online) Dispersion relations of the generalized SSH model with different hopping amplitude J: **(A)** $J = 0$; **(B)** $J/v = 1$; **(C)** $J/v = 1.8$; **(D)** $J/v = 2.5$. **(E–H)** The paths of the endpoint of the vector $\mathbf{d}(k)$ corresponding to **(A–D)** are shown on the d_x, d_y plane as the wavenumber is swept across the Brillouin zone, $k = 0 \to 2\pi$. The other parameters are $z/v = 0.8$ and $\phi = 0$.
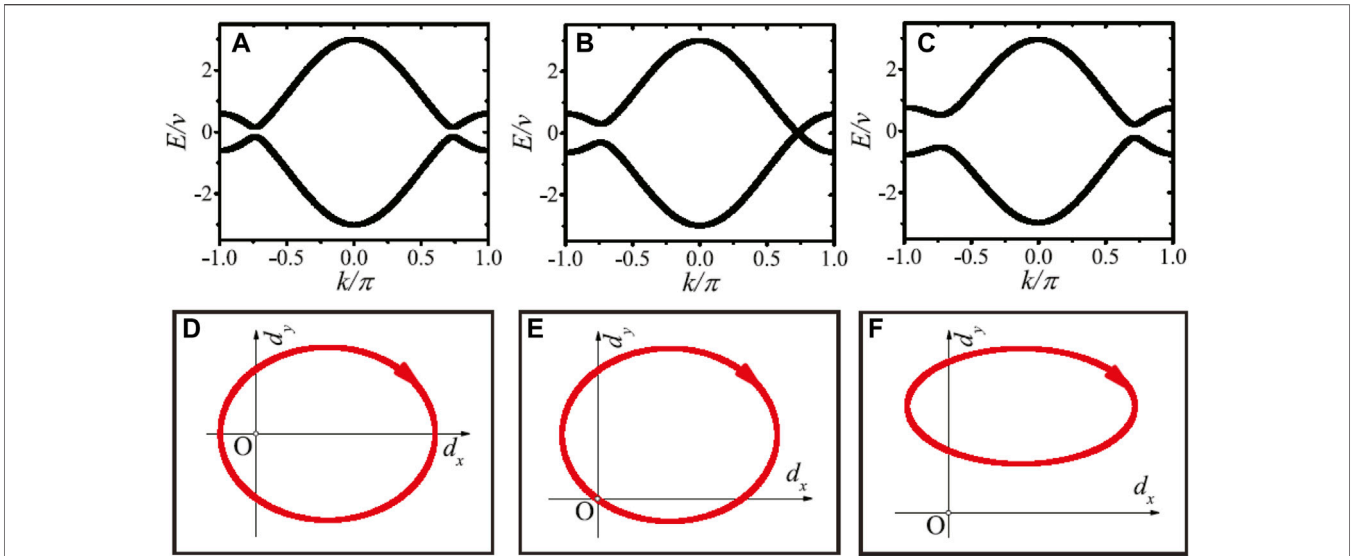
FIGURE 4 | (Color online) Dispersion relations of the generalized SSH model for hopping amplitude $J/v = 1.2$ with different phase: **(A)** $\phi = 0$; **(B)** $\phi = \phi_c \approx 0.04$; **(C)** $\phi = 0.1$. **(D–F)** The paths of the endpoint of the vector $\mathbf{d}(k)$, corresponding to **(A–C)**, are shown on the d_x, d_y plane as the wavenumber is swept across the Brillouin zone, $k = 0 \rightarrow 2\pi$. The other parameter is $z/v = 0.8$.

symmetry of the path about the d_x-axis is broken. The topological phase transition appears when $E = 0$, as shown in **Figure 4B**, which gives the critical phase ϕ_c as

$$\tan \phi_c = \frac{z - v}{z + v} \tan k, \qquad (20)$$

where

$$\cos^2 k = \frac{J^2 - (z - v)^2}{(z + v)^2 - (z - v)^2}. \qquad (21)$$

As $v > z$, we have $W = -1$ for $\phi = 0$ in **Figure 4A**; we have $W = 0$ for $\phi = 0.1$ in **Figure 4C**; the winding number is not well-defined at the critical point for $\phi = \phi_c \approx 0.04$ as shown in **Figure 4B**. On the contrary, see **Supplementary Figure S3** in the supplementary material [97], if $v < z$, we have $W = 1$ for $\phi = 0$; we have $W = 0$ for $\phi = 0.3$; there is no well-defined winding number at the critical point $\phi = \phi_c \approx 0.12$. The paths [see **Figures 4D–F** and **Supplementary Figures S3D,F**] that the endpoint of the vector $\mathbf{d}(k)$ traces, corresponding to dispersion relation [see **Figures 4A–C** and **Supplementary Figures S3A,C**], show the phase transition from $W = \pm 1$ to $W = 0$ by tuning ϕ.

4 EDGE STATES

We now study how to demonstrate topologically protected edge states in the optomechanical array of an open chain under single-particle excitation. To be specific, we propose an optomechanical array of an open chain for $N = 8$, then the wave function for the Hamiltonian in **Eq. 8** under single-particle excitation can be defined as

$$|\Psi(t)\rangle = \sum_{j=1}^{N} \left[c_{2j-1}(t) |a_j\rangle + c_{2j}(t) |b_j\rangle \right], \qquad (22)$$
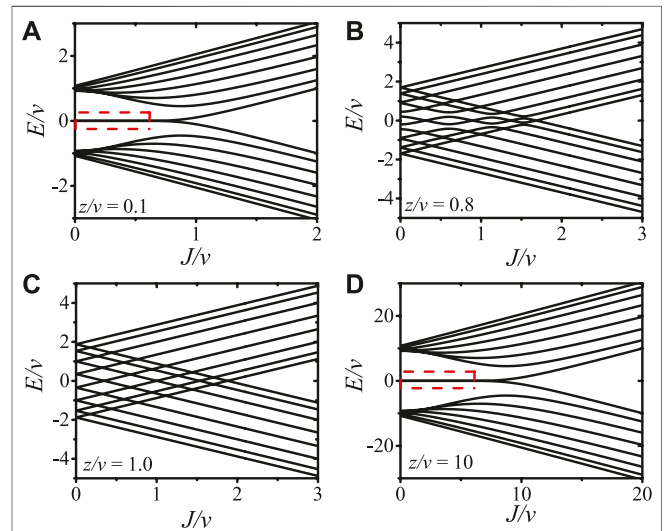

FIGURE 5 | (Color online) Energy spectrum of the open chain optomechanical array for $N = 8$ as a function the intracell hopping amplitude J for different intercell hopping amplitude z: **(A)** $z/v = 0.1$; **(B)** $z/v = 0.8$; **(C)** $z/v = 1.0$; **(D)** $z/v = 10$. The phase factor is $\phi = 0$.

where $P_{2j-1}(t) = |c_{2j-1}(t)|^2$ and $P_{2j}(t) = |c_{2j}(t)|^2$ denote the occupying probabilities in the jth cavity mode and jth mechanical mode, respectively. For simplicity, we define $P_i(t) = |c_i(t)|^2$ with the position index i, shown in **Figure 1**.

The energy spectrum of a generalized SSH model for $N = 8$ is shown in **Figure 5**. Under the conditions $z \ll v$ or $z \gg v$, see **Figures 5A,D**, the energy spectrum of a generalized SSH model is similar to that of the standard SSH model. However, due to the level crossings for the nearest neighbor eigenmodes and avoided
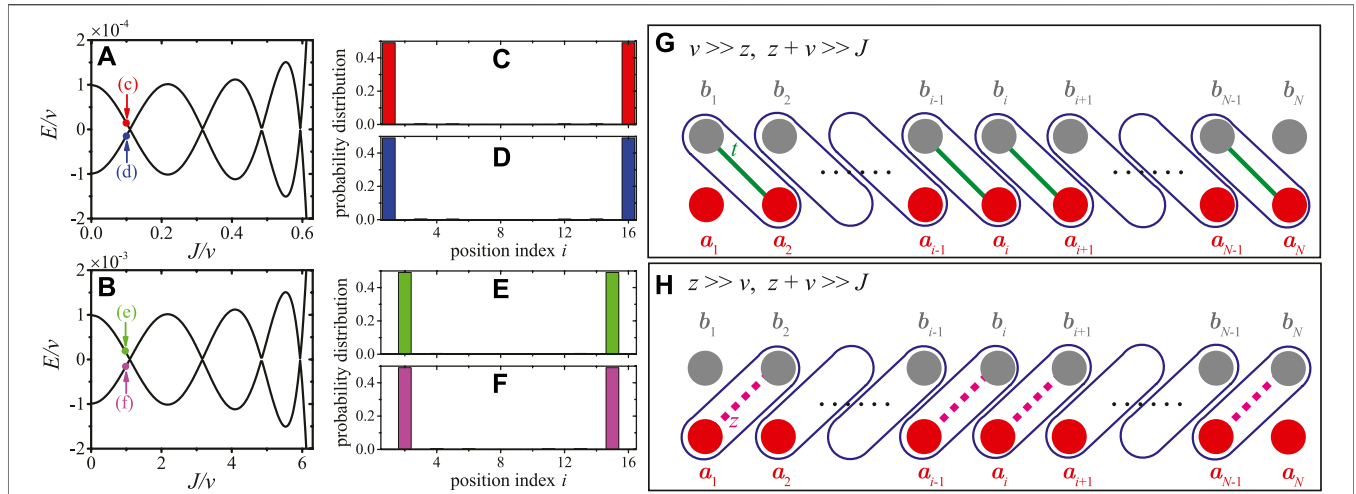
FIGURE 6 | (Color online) **(A, b)** are the local enlarged drawings of (**Figures 5A, D**). **(C–F)** show the probability distributions of the eigenfunctions corresponding to the points shown in **(A, B)**. **(G)** Edge states appear at a_1 and b_N corresponding to **(C, D)** for $v \gg z$ and $J \ll v + z$. **(H)** Edge states appear at b_1 and a_N corresponding to **(E, F)** for $z \gg v$ and $J \ll v + z$.

level crossings for the next-nearest neighbor eigenmodes, there are four ($N/2$) degenerate points of the zero-energy modes within the interval $0 < J < z + v$, as shown in **Figures 6A,B**, which are the local enlarged drawings of the boxes with red dashed-line in **Figures 5A,D**. When $z = 0.8v$, as shown **Figure 5B**, there are degenerate points for the nearest neighbor eigenmodes and avoided level crossings for the next-nearest neighbor eigenmodes. But when $z = v$, as shown **Figure 5C**, all the avoided level crossings for the next-nearest neighbor eigenmodes disappear.

The probability distributions of the eigenstates, corresponding to the points marked in **Figures 6A,B**, are shown in **Figures 6C–F**. It is obvious that the probability distributions of the eigenstates are localized. We define four edge states, i.e., left cavity (LC), left mechniacal (LM), right cavity (RC), right mechniacal (RM) edge states, as

$$|LC\rangle = \sum_{j=1}^{N} c_1 e^{-2(j-1)/\xi} |a_j\rangle, \qquad (23)$$

$$|LM\rangle = \sum_{j=1}^{N} c_2 e^{-2(j-1)/\xi} |b_j\rangle, \qquad (24)$$
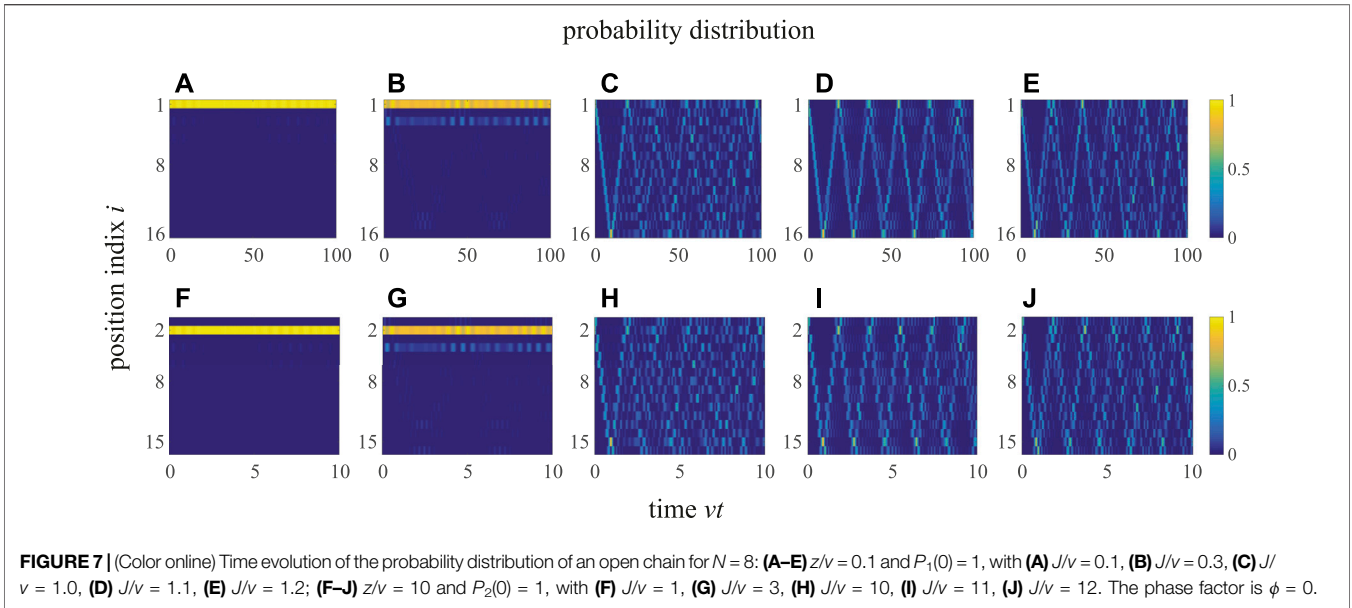
$$|RC\rangle = \sum_{j=1}^{N} c_{2N-1} e^{2(j-N)/\xi} |a_j\rangle, \qquad (25)$$

$$|RM\rangle = \sum_{j=1}^{N} c_{2N} e^{2(j-N)/\xi} |b_j\rangle, \qquad (26)$$

where $\xi > 0$ is the localization length determined by the amplitudes of v, z, and J. When $v \gg z$ and $J \ll v + z$ (corresponding to the winding number $W = -1$ under the periodic boundary condition), as shown in **Figures 6C,D**, the edge states are the hybridized states of the LC edge state and RM edge state. A concise physical picture for the edge states with $v \gg z$ and $J \ll v + z$ is shown in **Figure 6G**, where dimers are formed between b_j and a_{j+1}, and a_1 and b_N are isolated from the others.

Similarly, when $v \ll z$ and $J \ll v + z$ (corresponding to the winding number $W = 1$ under the periodic boundary condition), the edge states are the hybridized states of the LM edge state and RC edge state, as shown in **Figures 6E,F**. The physical picture for the edge states with $v \ll z$ and $J \ll v + z$ is shown in **Figure 6H**, where dimers are formed between a_j and b_{j+1}, and b_1 and a_N are isolated from the others. When $J > v + z$ (corresponding to the winding number $W = 0$ under the periodic boundary condition), dimers are formed between a_j and b_j, and no modes are isolated from the others (the physical picture is not shown in the text). Thus, there is no edge state when $J > v + z$.

Figure 7 shows the time evolution of the probability distribution for the generalized SSH model with the open boundary condition (i.e., an open chain for $N = 8$). In **Figures 7A–E**, an excitation is injected at the first cavity mode $P_1(0) = 1$ for $z = v/10$, and in **Figures 7F–J**, an excitation is injected at the first mechanical mode $P_2(0) = 1$ for $z = 10v$. From these figures, we can find that: 1) When $J = z \ll v$ or $J = v \ll z$, as shown in **Figures 7A,F**, the excitation almost localizes in the injected cavity or mechanical mode like a soliton for a long time. With a larger value of J (still with $J < z + v$), as shown in **Figures 7B,G**, the excitation spreads to the nearest neighbor modes and the localization of the excitation becomes weaker. 2) When $J = z + v$ (i.e., the topological phase transition point), as shown in **Figures 7D,I**, the excitation, oscillating like a soliton, travels in the open chain and reflects back at the ends. The traveling speed (the period of oscillation) depends the hopping amplitudes: the excitation travels much faster in **Figure 7I** with $z/v = 10$ and $J/v = 11$ than in **Figure 7D** with $z/v = 0.1$ and $J/v = 1.1$. As J is away from the topological phase transition point ($J \neq z + v$), as shown in **Figures 7C,E** [or **Figures 7H,J**], the distribution of the traveling excitation disperses much faster than the case with $J = z + v$. That is, the excitation travels like a soliton with less dispersion in the open chain when the system works at the critical point $J = z + v$.

FIGURE 7 | (Color online) Time evolution of the probability distribution of an open chain for $N = 8$: **(A–E)** $z/v = 0.1$ and $P_1(0) = 1$, with **(A)** $J/v = 0.1$, **(B)** $J/v = 0.3$, **(C)** $J/v = 1.0$, **(D)** $J/v = 1.1$, **(E)** $J/v = 1.2$; **(F–J)** $z/v = 10$ and $P_2(0) = 1$, with **(F)** $J/v = 1$, **(G)** $J/v = 3$, **(H)** $J/v = 10$, **(I)** $J/v = 11$, **(J)** $J/v = 12$. The phase factor is $\phi = 0$.

5 ADIABATIC PARTICLE PUMPING

As discussed in the previous section, when the driving strengths $\Omega_{j,\sigma}$ and detunings $\Delta_{j,\sigma}$ ($\sigma = 0, \pm$) of the external lasers are constant, and as a result the parameters J, ϕ, z and v are time independent in the steady state, then an excitation injected at one edge will stay there like a stationary state for long. However, we will show that it is possible to transfer the edge states from one to another by adiabatic pumping with periodically modulated optomechanical array. The periodically modulated optomechanical array can be realized by modulating the strengths $\Omega_{j,\sigma}$ and detunings $\Delta_{j,\sigma}$ of the driving fields, so that the detuning between the cavity modes and mechanical modes $u(t)$ and the classical amplitude $\alpha_{j,\sigma}$ become time dependent. By solving the classical equation of motion under the condition that the modulation frequency ω is much lower than the mechanical resonant frequency $\omega_{m,j}$, the classical amplitude $\alpha_{j,\sigma}$ can be expressed approximately as

$$\alpha_{j,\sigma}(t) = -i \int_0^t \Omega_{j,\sigma}(\tau) e^{\left[\frac{\kappa_j}{2} + i\left(\omega_{c,j} - \omega_{j,\sigma}\right)\right](\tau - t)} d\tau. \tag{27}$$

Following the same approach used in **Section 2**, the linearized Hamiltonian of the periodically modulated optomechanical array is given by

$$H = \sum_{j=1}^{N} \left[\frac{u_a(t)}{2} a_j^\dagger a_j + \frac{u_b(t)}{2} b_j^\dagger b_j + J(t) a_j^\dagger b_j \right] + \sum_{j=1}^{N-1} \left[v(t) a_{j+1}^\dagger b_j + z(t) b_{j+1}^\dagger a_j \right] + \text{H.c.}, \tag{28}$$

where $J(t) e^{i\phi} \equiv g_{j,0} \alpha_{j,0}(t)$, $v(t) \equiv g_{j,-} \alpha_{j,-}(t)$, and $z(t) \equiv g_{j,+} \alpha_{j,+}(t)$. To detect the robustness of the adiabatic pumping, we will consider the disorder effect by adding normally distributed random fluctuations ϵ with zero mean value to $u_a(t)$, $u_b(t)$, $J(t)$, $v(t)$, and $z(t)$ in the numerical calculations.
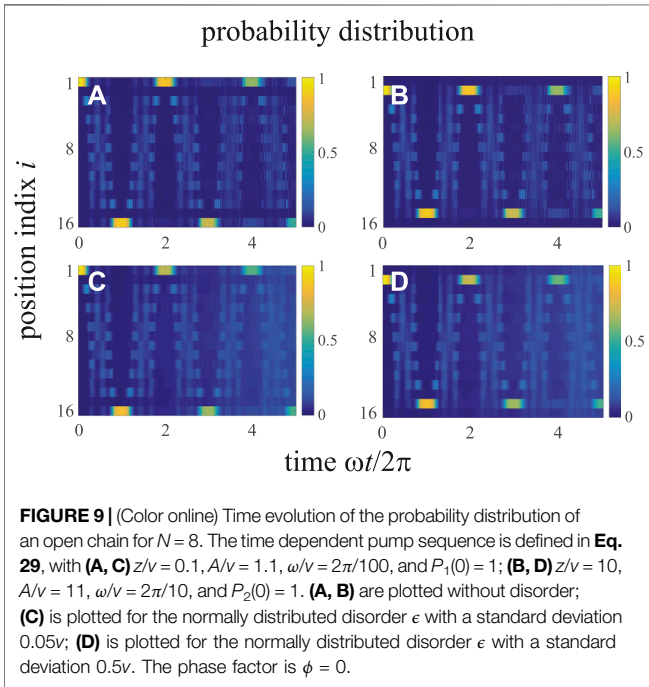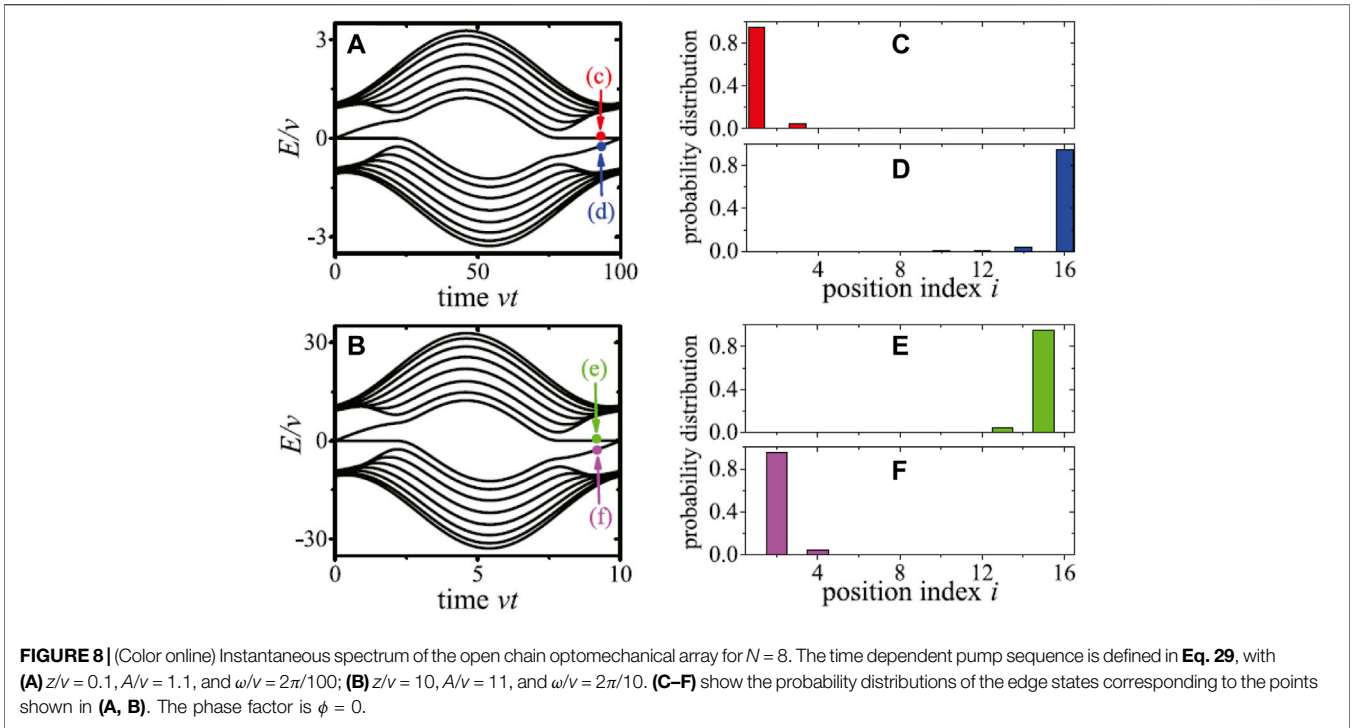
First, we consider a smooth modulation sequence as

$$\begin{cases} u_a(t) = \dfrac{A}{2} \sin(\omega t), \\ u_b(t) = 0, \\ J(t) = A[1 - \cos(\omega t)], \\ v(t) = \text{const.}, \\ z(t) = \text{const.}, \end{cases} \tag{29}$$

where, $u(t)$ and $J(t)$ are modulated periodically with amplitudes $A/2$ and A, and frequency ω; $u_b(t)$, $v(t)$, and $z(t)$ are constant.

The instantaneous spectrum of the Hamiltonian in **Eq. 28** with time dependent pump sequence defined in **Eq. 29** is shown in **Figures 8A,B**. In **Figures 8C–F**, the probability distributions of eigenstates corresponding to the points shown in **Figures 8A,B**, are approximately the edge states defined in **Eqs 23–26** as: **Figure 8C**, LC edge state; **Figure 8D**, RM edge state; **Figure 8E**, RC edge state; **Figure 8F**, LM edge state. When the adiabatic approximation holds, the system will stay in the same eigenstate. **Figure 8A** shows how a LC edge state is adiabatically pumped to the RM edge state during a pumping cycle, in the mean while **Figure 8B** shows how a RC edge state is adiabatically pumped to the LM edge state within a pumping cycle.

The dynamics of the probability distributions of an open chain with a time dependent pump sequence defined in **Eq. 29** is obtained numerically. As shown in **Figure 9A**, the excitation at the first cavity mode (LC edge state) quickly expands into the bulk, and then the probability distribution is concentrated around the Nth mechanical mode (RM edge state) at the end of the first pumping cycle. In the second pumping cycle, the excitation expands into the bulk again and concentrates on the first cavity mode (LC edge state) at the end of the second pumping cycle. Similarly, as shown in **Figure 9B**, the excitation at the first mechanical mode (LM edge state) expands into the bulk and

FIGURE 8 | (Color online) Instantaneous spectrum of the open chain optomechanical array for $N = 8$. The time dependent pump sequence is defined in **Eq. 29**, with **(A)** $z/v = 0.1$, $A/v = 1.1$, and $\omega/v = 2\pi/100$; **(B)** $z/v = 10$, $A/v = 11$, and $\omega/v = 2\pi/10$. **(C–F)** show the probability distributions of the edge states corresponding to the points shown in **(A, B)**. The phase factor is $\phi = 0$.

FIGURE 9 | (Color online) Time evolution of the probability distribution of an open chain for $N = 8$. The time dependent pump sequence is defined in **Eq. 29**, with **(A, C)** $z/v = 0.1$, $A/v = 1.1$, $\omega/v = 2\pi/100$, and $P_1(0) = 1$; **(B, D)** $z/v = 10$, $A/v = 11$, $\omega/v = 2\pi/10$, and $P_2(0) = 1$. **(A, B)** are plotted without disorder; **(C)** is plotted for the normally distributed disorder ϵ with a standard deviation $0.05v$; **(D)** is plotted for the normally distributed disorder ϵ with a standard deviation $0.5v$. The phase factor is $\phi = 0$.

concentrates on the Nth cavity mode (RC edge state) at the end of the first pumping cycle, and then the excitation expands into the bulk again and concentrates on the first mechanical mode (LM edge state) at the end of the second pumping cycle. These results are consistent with the instantaneous spectrum in the adiabatic limit, as shown in **Figure 8**. However, due to the Landau Zener transition, which occurs at the degenerate points $\omega t = 2n\pi$ (n is

positive integer), the periodical behavior of the probability distribution becomes less well-resolved in the following cycles. To prove that the adiabatically pumping is immune to small disorders, we re-plot **Figures 9A,B** in **Figures 9C,D** by adding the normally distributed disorder ϵ with a standard deviation 3) $0.05v$ and 4) $0.5v$. It is clear that **Figures 9C,D** are essentially identical to those in **Figures 9A,B**, i.e., the adiabatically pumping is robust against small disorders.

As shown in **Figures 8**, **9**, with time dependent pump sequence defined in **Eq. 29**, the LC edge state can be pumped adiabatically to the RM edge state, and the LM edge state can be pumped adiabatically to the RC edge state, and vice versa. However, the LC edge state cannot be pumped adiabatically to the RC edge state, and the LM edge state cannot be pumped adiabatically to the RM edge state. Now, we consider another smooth modulation sequence to realize the adiabatical pumping between the LC (LM) edge state and the RC (RM) edge state. The smooth modulation sequence is defined by

$$
\begin{cases}
u_a(t) = \dfrac{A}{2}\sin(\omega t), \\[2mm]
u_b(t) = 0, \\[2mm]
J(t) = \text{const.}, \\[2mm]
v(t) = A[1 + \cos(\omega t)], \\[2mm]
z(t) = A[1 - \cos(\omega t)].
\end{cases}
\tag{30}
$$

Here, $u(t)$, $v(t)$ and $z(t)$ are modulated periodically with amplitudes $A/2$ and A, and frequency ω, while $u_b(t) = 0$ and $J(t)$ is constant.

The instantaneous spectrum of the Hamiltonian in **Eq. 28** with time dependent pump sequence defined in **Eq. 30** is shown in
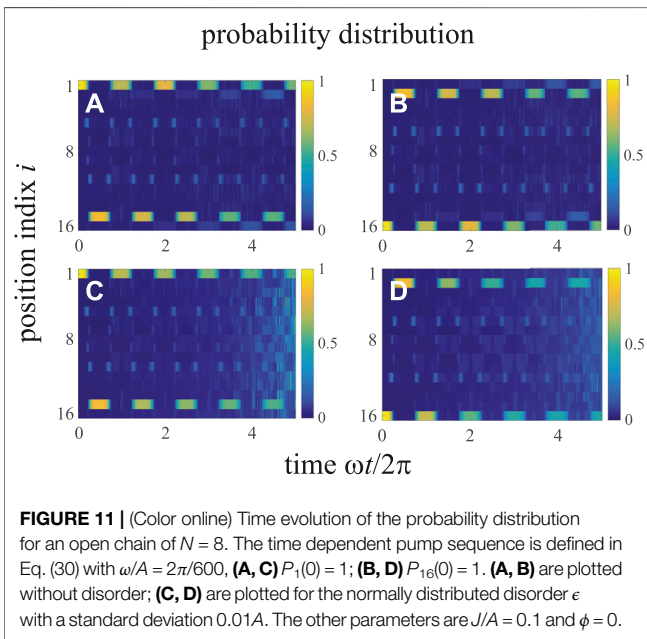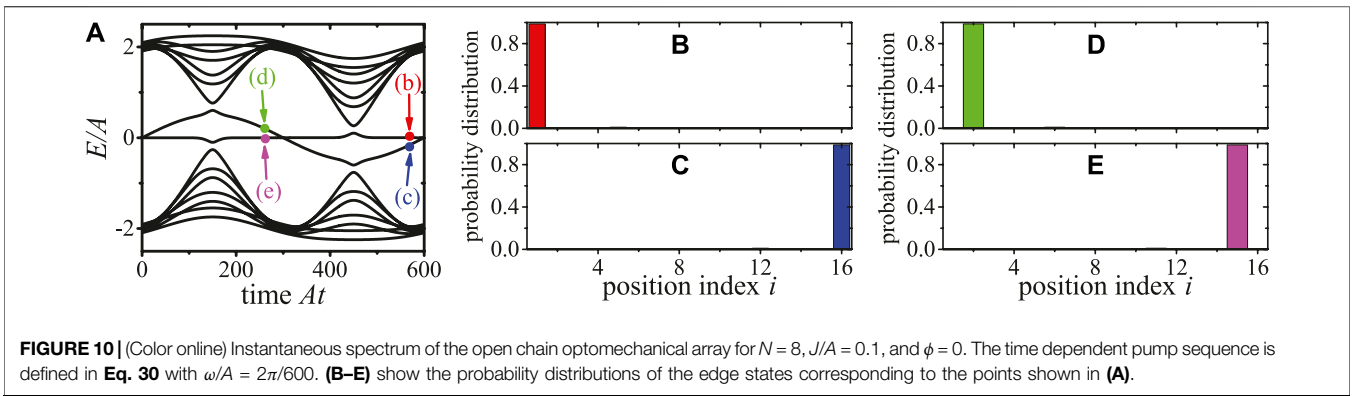
FIGURE 10 | (Color online) Instantaneous spectrum of the open chain optomechanical array for $N = 8$, $J/A = 0.1$, and $\phi = 0$. The time dependent pump sequence is defined in **Eq. 30** with $\omega/A = 2\pi/600$. **(B–E)** show the probability distributions of the edge states corresponding to the points shown in **(A)**.

FIGURE 11 | (Color online) Time evolution of the probability distribution for an open chain of $N = 8$. The time dependent pump sequence is defined in Eq. (30) with $\omega/A = 2\pi/600$, **(A, C)** $P_1(0) = 1$; **(B, D)** $P_{16}(0) = 1$. **(A, B)** are plotted without disorder; **(C, D)** are plotted for the normally distributed disorder ϵ with a standard deviation $0.01A$. The other parameters are $J/A = 0.1$ and $\phi = 0$.

Figure 10A. In **Figures 10B–E**, the probability distributions of eigenstates corresponding to the points shown in **Figure 10A**, are approximately the edge states defined in **Eqs 23–26** as: **Figure 10B** LC edge state; **Figure 10C** RM edge state; **Figure 10D** LM edge state; **Figure 10E** RC edge state. When the adiabatic approximation holds, the system will stay in the same eigenstate. **Figure 10A** shows how a LC edge state is adiabatically pumped to the RC edge state during a pumping cycle, in the mean while, a LM edge state is adiabatically pumped to the RM edge state within a pumping half-cycle.

The adiabatically pumping can also be studied directly by the dynamics of the probability distribution for an open chain with a time dependent pump sequence defined in **Eq. 30**. In **Figure 11A**, the excitation at the first cavity mode (LC edge state) quickly expands into the bulk, and then concentrates on the Nth cavity mode (RC edge state) at the end of the first pumping half-cycle. In the second pumping half-cycle, the excitation expands into the bulk again and concentrates on the first cavity mode (LC edge state) at the end of the first pumping cycle. Similarly, as shown in **Figure 11B**, the excitation at the first mechanical mode (LM edge

state) expands into the bulk and concentrates on the Nth mechanical mode (RM edge state) at the end of the first pumping half-cycle, and then the excitation expands into the bulk again and concentrates on the first mechanical mode (LM edge state) at the end of the first pumping cycle. However, the periodical behavior of the probability distribution becomes less well-resolved in the following cycles, which is induced by the Landau Zener transition at the degenerate points $\omega t = n\pi$ (n is positive integer). **Figures 11A,B** are re-plotted in **Figures 9C,D** for the normally distributed disorder ϵ with a standard deviation $0.01A$. Clearly, the adiabatically pumping is immune to the small disorders.

Overall, with time dependent pump sequence defined in **Eq. 29**, the LC edge state can be pumped adiabatically to the RM edge state, and the LM edge state can be pumped adiabatically to the RC edge state; with time dependent pump sequence defined in **Eq. 30**, the LC edge state can be pumped adiabatically to the RC edge state, and the LM edge state can be pumped adiabatically to the RM edge state. Therefore, the four edge states can be pumped from one to another adiabatically with smooth modulation sequence.

6 CONCLUSION

In summary, we have proposed to implement a generalized SSH model based on optomechanical arrays. This generalized SSH model supports two distinct nontrivial topological phases, and the transitions between different phases can be observed by tuning the strengths and phases of the effective optomechanical interactions. Dynamical control of the effective optomechanical interactions can be realized by tuning the strengths and phases of driving fields slowly, which allow for dynamical control of the topological phase transitions. Moreover, four types of edge states can be generated in the generalized SSH model of an open chain under single-particle excitation, and the dynamical behaviors of the excitation in the open chain depend on the topological properties under the periodic boundary condition. We show that the edge states can be pumped adiabatically along the optomechanical arrays by periodically modulating the amplitudes and frequencies of the driving fields, and the adiabatically pumping is immune to small disorders. Our results can be applied to control the transport of photons and phonons, and the generalized SSH model based

on the optomechanical arrays provides us a tunable platform to engineer topological phases for photons and phonons.

DATA AVAILABILITY STATEMENT

The original contributions presented in the study are included in the article/**Supplementary Material**, further inquiries can be directed to the corresponding authors.

AUTHOR CONTRIBUTIONS

X-WX, Y-JZ, and HW conceived the idea and X-WX carried out the calculation. X-WX, A-XC, and Y-XL supervised the work. All authors contributed to the interpretation of the work and the preparation of the manuscript.

FUNDING

SUPPLEMENTARY MATERIAL

The Supplementary Material for this article can be found online at: https://www.frontiersin.org/articles/10.3389/fphy.2021.813801/full#supplementary-material

Supplementary Figure S1 | (Color online) Dispersion relations of the generalized SSH model with different hopping amplitude J: **(A)** $J = 0$; **(B)** $J/v = 1$; **(C)** $J/v = 2$; **(D)** $J/v = 2.5$. **(E–H)** The paths of the endpoint of the vector d(k) corresponding to **(A–D)** are shown on the dx, dy plane as the wavenumber is swept across the Brillouin zone, $k = 0 \to 2\pi$. The other parameters are $z/v = 1$ and $\phi = 0$.

Supplementary Figure S2 | (Color online) Dispersion relations of the generalized SSH model with different hopping amplitude J: **(A)** $J = 0$; **(B)** $J/v = 1$; **(C)** $J/v = 2.2$; **(D)** $J/v = 2.7$. **(E–H)** The paths of the endpoint of the vector d(k) corresponding to **(A–D)** are shown on the dx, dy plane as the wavenumber is swept across the Brillouin zone, $k = 0 \to 2\pi$. The other parameters are $z/v = 1.2$ and $\phi = 0$.

Supplementary Figure S3 | (Color online) Dispersion relations of the generalized SSH model for hopping amplitude $J/v = 1.2$ with different phase: **(A)** $\phi = 0$; **(B)** $\phi = \phi c \approx 0.12$; **(C)** $\phi = 0.3$. **(D–F)** The paths of the endpoint of the vector d(k) corresponding to **(A–C)** are shown on the dx, dy plane as the wavenumber is swept across the Brillouin zone, $k = 0 \to 2\pi$. The other parameter is $z/v = 1.5$.

REFERENCES

1. Kippenberg TJ, Vahala KJ. Cavity Optomechanics: Back-Action at the Mesoscale. *Science* (2008) 321:1172–6. doi:10.1126/science.1156032
2. Marquardt F, Girvin S. Optomechanics. *Physics* (2009) 2:40. doi:10.1103/physics.2.40
3. Aspelmeyer M, Meystre P, Schwab K. Quantum Optomechanics. *Phys Today* (2012) 65(7):29–35. doi:10.1063/pt.3.1640
4. Aspelmeyer M, Kippenberg TJ, Marquardt F. Cavity Optomechanics. *Rev Mod Phys* (2014) 86:1391–452. doi:10.1103/revmodphys.86.1391
5. Metcalfe M. Applications of Cavity Optomechanics. *Appl Phys Rev* (2014) 1:031105. doi:10.1063/1.4896029
6. Liu Y-l., Wang C, Zhang J, Liu Y-x., Cavity Optomechanics: Manipulating Photons and Phonons towards the Single-Photon strong Coupling. *Chin Phys. B* (2018) 27:024204. doi:10.1088/1674-1056/27/2/024204
7. Lin Q, Rosenberg J, Jiang X, Vahala KJ, Painter O. Mechanical Oscillation and Cooling Actuated by the Optical Gradient Force. *Phys Rev Lett* (2009) 103:103601. doi:10.1103/physrevlett.103.103601
8. Li M, Pernice WHP, Tang HX. Tunable Bipolar Optical Interactions between Guided Lightwaves. *Nat Photon* (2009) 3:464–8. doi:10.1038/nphoton.2009.116
9. Weis S, Rivière R, Deléglise S, Gavartin E, Arcizet O, Schliesser A, et al. Optomechanically Induced Transparency. *Science* (2010) 330:1520–3. doi:10.1126/science.1195596
10. Zhang M, Shah S, Cardenas J, Lipson M. Synchronization and Phase Noise Reduction in Micromechanical Oscillator Arrays Coupled through Light. *Phys Rev Lett* (2015) 115:163902. doi:10.1103/physrevlett.115.163902
11. Teufel JD, Li D, Allman MS, Cicak K, Sirois AJ, Whittaker JD, et al. Circuit Cavity Electromechanics in the strong-coupling Regime. *Nature* (2011) 471:204–8. doi:10.1038/nature09898
12. Massel F, Cho SU, Pirkkalainen J-M, Hakonen PJ, Heikkilä TT, Sillanpää MA. Multimode Circuit Optomechanics Near the Quantum Limit. *Nat Commun* (2012) 3:987. doi:10.1038/ncomms1993
13. Palomaki TA, Teufel JD, Simmonds RW, Lehnert KW. Entangling Mechanical Motion with Microwave Fields. *Science* (2013) 342:710–3. doi:10.1126/science.1244563

14. Suh J, Weinstein AJ, Lei CU, Wollman EE, Steinke SK, Meystre P, et al. Mechanically Detecting and Avoiding the Quantum Fluctuations of a Microwave Field. *Science* (2014) 344:1262–5. doi:10.1126/science.1253258
15. Eichenfield M, Chan J, Camacho RM, Vahala KJ, Painter O. Optomechanical Crystals. *Nature* (2009) 462:78–82. doi:10.1038/nature08524
16. Safavi-Naeini AH, Hill JT, Meenehan S, Chan J, Gröblacher S, Painter O. Two-Dimensional Phononic-Photonic Band Gap Optomechanical Crystal Cavity. *Phys Rev Lett* (2014) 112:153603. doi:10.1103/physrevlett.112.153603
17. Chang DE, Safavi-Naeini AH, Hafezi M, Painter O. Slowing and Stopping Light Using an Optomechanical crystal Array. *New J Phys* (2011) 13:23003. doi:10.1088/1367-2630/13/2/023003
18. Chen W, Clerk AA. Photon Propagation in a One-Dimensional Optomechanical Lattice. *Phys Rev A* (2014) 89:033854. doi:10.1103/physreva.89.033854
19. Heinrich G, Ludwig M, Qian J, Kubala B, Marquardt F. Collective Dynamics in Optomechanical Arrays. *Phys Rev Lett* (2011) 107:043603. doi:10.1103/PhysRevLett.107.043603
20. Ludwig M, Marquardt F. Quantum Many-Body Dynamics in Optomechanical Arrays. *Phys Rev Lett* (2013) 111:073603. doi:10.1103/PhysRevLett.111.073603
21. Lauter R, Mitra A, Marquardt F. From Kardar-Parisi-Zhang Scaling to Explosive Desynchronization in Arrays of Limit-Cycle Oscillators. *Phys Rev E* (2017) 96:012220. doi:10.1103/PhysRevE.96.012220
22. Schmidt M, Kessler S, Peano V, Painter O, Marquardt F. Optomechanical Creation of Magnetic fields for Photons on a Lattice. *Optica* (2015) 2:635. doi:10.1364/optica.2.000635
23. Schmidt M, Peano V, Marquardt F. (2013) *Optomechanical Metamaterials: Dirac Polaritons, Gauge fields, and Instabilities*. arXiv:1311.7095 [physics.optics].
24. Schmidt M, Peano V, Marquardt F. Optomechanical Dirac Physics. *New J Phys* (2015) 17:023025. doi:10.1088/1367-2630/17/2/023025
25. Roque TF, Peano V, Yevtushenko OM, Marquardt F. Anderson Localization of Composite Excitations in Disordered Optomechanical Arrays. *New J Phys* (2017) 19:013006. doi:10.1088/1367-2630/aa52e2
26. Wan L-L, Lü X-Y, Gao J-H, Wu Y. Controllable Photon and Phonon Localization in Optomechanical Lieb Lattices. *Opt Express* (2017) 25:17364. doi:10.1364/oe.25.017364

27. Xiong H, Gan J, Wu Y. Kuznetsov-Ma Soliton Dynamics Based on the Mechanical Effect of Light. *Phys Rev Lett* (2017) 119:153901. doi:10.1103/physrevlett.119.153901

28. Peano V, Brendel C, Schmidt M, Marquardt F. Topological Phases of Sound and Light. *Phys Rev X* (2015) 5:031011. doi:10.1103/physrevx.5.031011

29. Peano V, Houde M, Marquardt F, Clerk AA. Topological Quantum Fluctuations and Traveling Wave Amplifiers. *Phys Rev X* (2016) 6:041026. doi:10.1103/physrevx.6.041026

30. Peano V, Houde M, Brendel C, Marquardt F, Clerk AA. Topological Phase Transitions and Chiral Inelastic Transport Induced by the Squeezing of Light. *Nat Commun* (2016) 7:10779. doi:10.1038/ncomms10779

31. Minkov M, Savona V. Haldane Quantum Hall Effect for Light in a Dynamically Modulated Array of Resonators. *Optica* (2016) 3:200. doi:10.1364/optica.3.000200

32. Brendel C, Peano V, Painter O, Marquardt F. Snowflake Phononic Topological Insulator at the Nanoscale. *Phys Rev B* (2018) 97:020102(R). doi:10.1103/physrevb.97.020102

33. Qi L, Xing Y, Wang H-F, Zhu A-D, Zhang S. Simulating Z_2 Topological Insulators via a One-Dimensional Cavity Optomechanical Cells Array. *Opt Express* (2017) 25:17948. doi:10.1364/oe.25.017948

34. Xing Y, Qi L, Cao J, Wang D-Y, Bai C-H, Cui W-X, et al. Controllable Photonic and Phononic Edge Localization via Optomechanically Induced Kitaev Phase. *Opt Express* (2018) 26:16250. doi:10.1364/oe.26.016250

35. Heeger AJ, Kivelson S, Schrieffer JR, Su W-P. Solitons in Conducting Polymers. *Rev Mod Phys* (1988) 60:781–850. doi:10.1103/revmodphys.60.781

36. Bermudez A, Schaetz T, Porras D. Photon-Assisted-Tunneling Toolbox for Quantum Simulations in Ion Traps. *New J Phys* (2012) 14:053049. doi:10.1088/1367-2630/14/5/053049

37. Atala M, Aidelsburger M, Barreiro JT, Abanin D, Kitagawa T, Demler E, et al. Direct Measurement of the Zak Phase in Topological Bloch Bands. *Nat Phys* (2013) 9:795–800. doi:10.1038/nphys2790

38. Goldman N, Juzeliūnas G, Öhberg P, Spielman IB. Light-Induced Gauge Fields for Ultracold Atoms. *Rep Prog Phys* (2014) 77:126401. doi:10.1088/0034-4885/77/12/126401

39. Jotzu G, Messer M, Desbuquois R, Lebrat M, Uehlinger T, Greif D, et al. Experimental Realization of the Topological Haldane Model with Ultracold Fermions. *Nature* (2014) 515:237–40. doi:10.1038/nature13915

40. Duca L, Li T, Reitter M, Bloch I, Schleier-Smith M, Schneider U. An Aharonov-Bohm Interferometer for Determining Bloch Band Topology. *Science* (2015) 347:288–92. doi:10.1126/science.1259052

41. Engelhardt G, Brandes T. Topological Bogoliubov Excitations in Inversion-Symmetric Systems of Interacting Bosons. *Phys Rev A* (2015) 91:053621. doi:10.1103/physreva.91.053621

42. Engelhardt G, Benito M, Platero G, Brandes T. Topological Instabilities in Ac-Driven Bosonic Systems. *Phys Rev Lett* (2016) 117:045302. doi:10.1103/PhysRevLett.117.045302

43. Nakajima S, Tomita T, Taie S, Ichinose T, Ozawa H, Wang L, et al. Topological Thouless Pumping of Ultracold Fermions. *Nat Phys* (2016) 12:296–300. doi:10.1038/nphys3622

44. Lohse M, Schweizer C, Zilberberg O, Aidelsburger M, Bloch I. A Thouless Quantum Pump with Ultracold Bosonic Atoms in an Optical Superlattice. *Nat Phys* (2016) 12:350–4. doi:10.1038/nphys3584

45. Meier EJ, An FA, Gadway B. Observation of the Topological Soliton State in the Su-Schrieffer-Heeger Model. *Nat Commun* (2016) 7:13986. doi:10.1038/ncomms13986

46. Song B, Zhang L, He C, Poon TFJ, Hajiyev E, Zhang S, et al. Observation of Symmetry-Protected Topological Band with Ultracold Fermions. *Sci Adv* (2018) 4:eaao4748. doi:10.1126/sciadv.aao4748

47. Lu L, Joannopoulos JD, Soljačić M. Topological Photonics. *Nat Photon* (2014) 8:821–9. doi:10.1038/nphoton.2014.248

48. Lu L, Joannopoulos JD, Soljačić M. Topological States in Photonic Systems. *Nat Phys* (2016) 12:626–9. doi:10.1038/nphys3796

49. Khanikaev AB, Shvets G. Two-dimensional Topological Photonics. *Nat Photon* (2017) 11:763–73. doi:10.1038/s41566-017-0048-5

50. Sun X-C, He C, Liu X-P, Lu M-H, Zhu S-N, Chen Y-F. Two-dimensional Topological Photonic Systems. *Prog Quan Electron* (2017) 55:52–73. doi:10.1016/j.pquantelec.2017.07.004

51. Ozawa T, Price HM, Amo A, Goldman N, Hafezi M, Lu L, et al. 2018 *Topological Photonics*. arXiv:1802.04173 [physics.optics].

52. Fleury R, Sounas D, R Haberman M, Alù A. *Nonreciprocal actoustics, Acoust Today* (2015) 11:14.

53. Huber SD. Topological Mechanics. *Nat Phys* (2016) 12:621–3. doi:10.1038/nphys3801

54. Xiao M, Ma G, Yang Z, Sheng P, Zhang ZQ, Chan CT. Geometric Phase and Band Inversion in Periodic Acoustic Systems. *Nat Phys* (2015) 11:240–4. doi:10.1038/nphys3228

55. Belopolski I, Xu SY, Koirala N, Liu C, Bian G, Strocov VN, et al. A Novel Artificial Condensed Matter Lattice and a New Platform for One-Dimensional Topological Phases. *Sci Adv* (2017) 3:e1501692. doi:10.1126/sciadv.1501692

56. Gröning O, Wang S, Yao X, Pignedoli CA, Borin Barin G, Daniels C, et al. Engineering of Robust Topological Quantum Phases in Graphene Nanoribbons. *Nature* (2018) 560:209–13. doi:10.1038/s41586-018-0375-9

57. Poddubny A, Miroshnichenko A, Slobozhanyuk A, Kivshar Y. Topological Majorana States in Zigzag Chains of Plasmonic Nanoparticles. *ACS Photon* (2014) 1:101–5. doi:10.1021/ph4000949

58. Cheng Q, Pan Y, Wang Q, Li T, Zhu S. Topologically Protected Interface Mode in Plasmonic Waveguide Arrays. *Laser Photon Rev* (2015) 9:392–8. doi:10.1002/lpor.201400462

59. Ge L, Wang L, Xiao M, Wen W, Chan CT, Han D. Topological Edge Modes in Multilayer Graphene Systems. *Opt Express* (2015) 23:21585. doi:10.1364/oe.23.021585

60. Ling CW, Xiao M, Chan CT, Yu SF, Fung KH. Topological Edge Plasmon Modes between Diatomic Chains of Plasmonic Nanoparticles. *Opt Express* (2015) 23:2021. doi:10.1364/oe.23.002021

61. Liu C, Gurudev Dutt MV, Pekker D. Robust Manipulation of Light Using Topologically Protected Plasmonic Modes. *Opt Express* (2018) 26:2857–72. doi:10.1364/OE.26.002857

62. Downing CA, Weick G. Topological Collective Plasmons in Bipartite Chains of Metallic Nanoparticles. *Phys Rev B* (2017) 95:125426. doi:10.1103/physrevb.95.125426

63. Downing CA, Weick G. (2018) *Topological Plasmons in Dimerized Chains of Nanoparticles: Robustness against Long-Range Quasistatic Interactions and Retardation Effects*. arXiv:1803.08872 [cond-mat.mes-hall].

64. Koch J, Houck AA, Hur KL, Girvin SM. Time-reversal-symmetry Breaking in Circuit-QED-Based Photon Lattices. *Phys Rev A* (2010) 82:043811. doi:10.1103/physreva.82.043811

65. Nunnenkamp A, Koch J, Girvin SM. Synthetic Gauge fields and Homodyne Transmission in Jaynes-Cummings Lattices. *New J Phys* (2011) 13:095008. doi:10.1088/1367-2630/13/9/095008

66. Mei F, You JB, Nie W, Fazio R, Zhu SL, Kwek LC. Simulation and Detection of Photonic Chern Insulators in a One-Dimensional Circuit-QED Lattice. *Phys Rev A* (2015) 92:041805(R). doi:10.1103/physreva.92.041805

67. Mei F, Xue Z-Y, Zhang D-W, Tian L, Lee C, Zhu S-L. Witnessing Topological Weyl Semimetal Phase in a Minimal Circuit-QED Lattice. *Quan Sci. Technol.* (2016) 1:015006. doi:10.1088/2058-9565/1/1/015006

68. Yang ZH, Wang YP, Xue ZY, Yang WL, Hu Y, Gao JH, et al. Circuit Quantum Electrodynamics Simulator of at Band Physics in a Lieb Lattice. *Phys Rev A* (2016) 93:062319. doi:10.1103/physreva.93.062319

69. Engelhardt G, Benito M, Platero G, Brandes T. Topologically Enforced Bifurcations in Superconducting Circuits. *Phys Rev Lett* (2017) 118:197702. doi:10.1103/physrevlett.118.197702

70. Tangpanitanon J, Bastidas VM, Al-Assam S, Roushan P, Jaksch D, Angelakis DG. Topological Pumping of Photons in Nonlinear Resonator Arrays. *Phys Rev Lett* (2016) 117:213603. doi:10.1103/physrevlett.117.213603

71. Gu X, Chen S, Liu YX, (2017) *Topological Edge States and Pumping in a Chain of Coupled Superconducting Qubits*. arXiv:1711.06829v1 [quant-ph].

72. Clay RT, Mazumdar S. Cooperative Density Wave and Giant Spin Gap in the Quarter-Filled Zigzag Electron Ladder. *Phys Rev Lett* (2005) 94:207206. doi:10.1103/physrevlett.94.207206

73. Li X, Zhao E, Vincent Liu W. Topological States in a Ladder-like Optical Lattice Containing Ultracold Atoms in Higher Orbital Bands. *Nat Commun* (2013) 4:1523. doi:10.1038/ncomms2523

74. Shimizu Y, Aoyama S, Jinno T, Itoh M, Ueda Y. Site-Selective Mott Transition in a Quasi-One-Dimensional VanadateV6O13. *Phys Rev Lett* (2015) 114: 166403. doi:10.1103/physrevlett.114.166403

75. Cheon S, Kim T-H, Lee S-H, Yeom HW. Chiral Solitons in a Coupled Double Peierls Chain. *Science* (2015) 350:182–5. doi:10.1126/science.aaa7055

76. Zhang T, Jo G-B. One-dimensional Sawtooth and Zigzag Lattices for Ultracold Atoms. *Sci Rep* (2015) 5:16044. doi:10.1038/srep16044

77. Li C, Lin S, Zhang G, Song Z. Topological Nodal Points in Two Coupled Su-Schrieffer-Heeger Chains. *Phys Rev B* (2017) 96:125418. doi:10.1103/physrevb.96.125418

78. Asbóth JK, Oroszlány L, Pályi A. *A Short Course on Topological Insulators*. In: *Lecture Notes in Physics*, 919. Cham: Springer International Publishing (2016). doi:10.1007/978-3-319-25607-8

79. Znojil M. Novel Recurrent Approach to the Generalized Su-Schrieffer-Heeger Hamiltonians. *Phys Rev B* (1989) 40:12468–75. doi:10.1103/physrevb.40.12468

80. Li L, Xu Z, Chen S. Topological Phases of Generalized Su-Schrieffer-Heeger Models. *Phys Rev B* (2014) 89:085111. doi:10.1103/physrevb.89.085111

81. Zeng Q-B, Chen S, Lü R. Generalized Aubry-André-Harper Model Withp-Wave Superconducting Pairing. *Phys Rev B* (2016) 94:125408. doi:10.1103/physrevb.94.125408

82. Longhi S. Topological Pumping of Edge States via Adiabatic Passage. *Phys Rev B* (2019) 99:155150. doi:10.1103/physrevb.99.155150

83. Du L, Wu JH, Artoni M, La Rocca GC. Phase-dependent Topological Interface State and Spatial Adiabatic Passage in a Generalized Su-Schrieffer-Heeger Model. *Phys Rev A* (2019) 100:012112. doi:10.1103/physreva.100.012112

84. Du L, Wu JH, Artoni M, La Rocca GC. Fractional Quantum Transport and Staggered Topological Transition in a Lossy Trimerized Lattice. *Phys Rev A* (2019) 100:052102. doi:10.1103/physreva.100.052102

85. Ahmadi N, Abouie J, Baeriswyl D. Topological and Nontopological Features of Generalized Su-Schrieffer-Heeger Models. *Phys Rev B* (2020) 101:195117. doi:10.1103/physrevb.101.195117

86. Xu XW, Zhao YJ, Wang H, Chen AX, Liu YX. (2018) *Generalized Su-Schrieffer-Heeger Model in One Dimensional Optomechanical Arrays*. arXiv:1807.07880.

87. Qi L, Wang G-L, Liu S, Zhang S, Wang H-F. Engineering the Topological State Transfer and Topological Beam Splitter in an Even-Sized Su-Schrieffer-Heeger Chain. *Phys Rev A* (2020) 102:022404. doi:10.1103/physreva.102.022404

88. Cao J, Cui W-X, Yi XX, Wang H-F. Controllable Photon-Phonon Conversion via the Topologically Protected Edge Channel in an Optomechanical Lattice. *Phys Rev A* (2021) 103:023504. doi:10.1103/physreva.103.023504

89. Ni X, Kim S, Alù A. Topological Insulator in Two Synthetic Dimensions Based on an Optomechanical Resonator. *Optica* (2021) 8:1024. doi:10.1364/optica.430821

90. Mathew JP, Pino Jd., Verhagen E. Synthetic Gauge fields for Phonon Transport in a Nano-Optomechanical System. *Nat Nanotechnol* (2020) 15:198–202. doi:10.1038/s41565-019-0630-8

91. Safavi-Naeini AH, Chan J, Hill JT, Gröblacher S, Miao H, Chen Y, et al. Laser Noise in Cavity-Optomechanical Cooling and Thermometry. *New J Phys* (2013) 15:035007. doi:10.1088/1367-2630/15/3/035007

92. Kronwald A, Marquardt F, Clerk AA. Arbitrarily Large Steady-State Bosonic Squeezing via Dissipation. *Phys Rev A* (2013) 88:063833. doi:10.1103/physreva.88.063833

93. Xu XW, Li Y, Chen AX, Liu YX. Nonreciprocal Conversion between Microwave and Optical Photons in Electro-Optomechanical Systems. *Phys Rev A* (2016) 93:023827. doi:10.1103/physreva.93.023827

94. Peterson GA, Lecocq F, Cicak K, Simmonds RW, Aumentado J, Teufel JD. Demonstration of Efficient Nonreciprocity in a Microwave Optomechanical Circuit. *Phys Rev X* (2017) 7:031001. doi:10.1103/physrevx.7.031001

95. Bernier NR, Tóth LD, Koottandavida A, Ioannou MA, Malz D, Nunnenkamp A, et al. Nonreciprocal Reconfigurable Microwave Optomechanical Circuit. *Nat Commun* (2017) 8:604. doi:10.1038/s41467-017-00447-1

96. Barzanjeh S, Wulf M, Peruzzo M, Kalaee M, Dieterle PB, Painter O, et al. Mechanical On-Chip Microwave Circulator. *Nat Commun* (2017) 8:953. doi:10.1038/s41467-017-01304-x